

Electrochemical Corrosion and Tribocorrosion Properties of Sol-Gel ZrO₂ Films Coated on Stainless Steel in the Diverse NaCl Aqueous Solutions

Zhang Zhenhua, Ji Guojun

College of Chemical Engineering, Inner Mongolia University of Technology, Hohhot 010051, China

Abstract: ZrO₂ films were deposited on 304 stainless-steel substrates by a sol-gel spin coating method. Electrochemical testing technology and a to-and-fro wear test apparatus were used to study the electrochemical corrosion and tribocorrosion properties of the films in different NaCl solutions. According to the results, the coated specimens are better than the bare matrix in resistance to corrosion and tribocorrosion. In the NaCl solutions, increasing either the solution temperature or concentration decreases the protective effects of the ZrO₂ films; study of the solution temperature factor show that serious pitting corrosion and obvious cracking occur on the surface of the coated specimens; study of the solution concentration factor show pitting corrosion on the sample surfaces. Regarding the tribocorrosion of the coated specimens, as the NaCl concentration increases from 2% to 6.5%, the abrasive wear is more obvious, and the corrosive wear is aggravated.

Key words: ZrO₂ films; NaCl solution; electrochemical corrosion; tribocorrosion

With the modern development of industrial science and technology, steel has been extensively applied in all fields of industrial production and national life due to the mature processing and manufacturing technology for steel with excellent physical and chemical properties. Steel has become one of the most important engineering materials in national production and life^[1]. Among the types of steel, stainless steel has excellent mechanical properties and broad applications^[2-4]. Accordingly, 304 stainless steels are widely used in certain equipment exposed to corrosion by virtue of the low price, good comprehensive mechanical performance and high corrosion resistance of this material. However, the further use of 304 stainless steel is restricted by low hardness and poor wear resistance^[5]. Moreover, in corrosive environments, wear and corrosion are the main forms of material failure, resulting in material degradation, especially in an environment containing chloride ions. With the mutual effects of wear and corrosion in a corrosive environment, tribocorrosion also occurs on the working surface^[6]. Problems with tribocorrosion are encountered in

processes such as those in chemical, aerospace, marine^[7], biomedical, and automotive applications^[8]. In view of these problems, a surface treatment is generally required to improve the surface performance of the material; thus, ceramic coatings are deposited on stainless-steel surfaces in many studies to account for insufficient surface performance^[9-11].

The related literature reports that oxide ceramic coatings can improve the wear resistance and corrosion resistance of metals^[12]. Moreover, ceramics and ceramic coatings generally have good passivity, which are insulators or have low conductivity and exhibit good corrosion resistance in corrosive media^[13]. Among the ceramics used, ZrO₂ is a special ceramic material with high ionic conductivity, low thermal conductivity, and good mechanical strength and corrosion resistance^[14-16], and the thermal expansion coefficient of ZrO₂ closely matches those of most metals^[17], which can reduce surface crack formation during the high temperature sintering of thin films. ZrO₂ has been widely studied due to its promising properties and has been exten-

Received date: November 12, 2019

Foundation item: National Natural Science Foundation of China (11462017)

Corresponding author: Ji Guojun, Ph. D., Professor, College of Chemical Engineering, Inner Mongolia University of Technology, Hohhot 010051, P. R. China, Tel: 0086-471-6575722, E-mail: jgj@imut.edu.cn

Copyright © 2020, Northwest Institute for Nonferrous Metal Research. Published by Science Press. All rights reserved.

sively applied, such as in capacitance sensors^[18], optical thin films^[19], high-temperature solid fuel cells^[20] and protective coatings^[21]. Furthermore, ZrO₂ is a promising candidate material as a protective coating for stainless steel^[22]. The related research shows that in a 3.5 wt% NaCl solution, the presence of a ZrO₂ film can reduce the corrosion current and provide a protective barrier for the substrate^[23]. Compared with a bare substrate, fewer exposed holes exist on the surface of a matrix coated with ZrO₂ thin films, and ZrO₂ films of monoclinic phase and tetragonal phase inhibit the ingress of corrosive ions^[24]. In addition, for NiTi alloys, the existence of a ZrO₂ coating can reportedly remarkably ameliorate the corrosion resistance of the alloy with decrease of the friction coefficient^[25]. A study of titanium matrices found that the addition of ZrO₂ decreases the friction coefficient under much higher loads and hence improves the wear performance of the matrix^[26]; with respect to material coatings, related research shows that the addition of ZrO₂ to Ti-Ni coatings noticeably improves the tribocorrosion properties of the coatings^[27]. Therefore, the tribocorrosion performance of ZrO₂ films requires further experiments and investigation; the tribocorrosion properties of these layers and metal-related materials are the subject of numerous studies, and these research studies are more significant because of the lack of studies on the corrosion-wear of ZrO₂ films. However, the properties of ZrO₂ films are limited by many factors. The physical and chemical properties of ZrO₂ films strongly rely on the deposition methods^[28]. The discrepancy in the corrosion resistances of ZrO₂ films prepared by different deposition methods is a critical issue that must be addressed. The methods used in the preparation of ZrO₂ films are mainly chemical vapor deposition^[29], sputtering^[30], ion-beam deposition^[31], plasma spraying^[32] and sol-gel spin coating^[33]. Sol-gel spin coating is an environmentally friendly method for the preparation of ZrO₂ thin films that has been widely used by researchers because this method is economical, convenient and easy to operate^[34-36].

Currently, a number of studies focus on the properties and characteristics of ZrO₂ films; moreover, the tribocorrosion properties of ZrO₂ composite materials prepared by different techniques are a concern of many researchers. However, few investigators have further studied the corrosion and tribocorrosion behaviors of ZrO₂ films prepared by the sol-gel spin coating process in different NaCl solutions. Accordingly, it is of great significance to study the electrochemical corrosion and tribocorrosion properties of ZrO₂ films prepared by the sol-gel spin coating method in different NaCl solutions for the improvement and advancement of the corrosion properties to provide a reliable basis for the accurate evaluation of the performance of ZrO₂ films. In this paper, ZrO₂ sols were prepared by a sol-gel process and then spin coated on a stainless steel surface.

Based on the solution temperature and concentration factors, the electrochemical corrosion and tribocorrosion behaviors of the coated specimens were studied in different NaCl solutions.

1 Experiment

1.1 Preparation and treatment of materials

In the present experiment, the matrix material used for sample preparation was 304 stainless steel sheets with a size of 20 mm × 10 mm × 1 mm that were produced by Taiyuan Iron and Steel Group Co. Ltd. Before deposition of the films, the mirror sides of the stainless steel sheets were cleaned in an ultrasonic bath and rinsed in distilled water. The sols needed for deposition were produced. Zr(OC₄H₉)₄ was used as a precursor for the preparation of the sols. As shown in Fig.1, 30 mL of ethanol was mixed with 8 mL of precursor, and then, 2.5 mL of anhydrous acetic acid was added during an agitation process of continuous stirring for 140 min, preparing the stable ZrO₂ sols. Combined with the sol-gel technology, as seen in Fig.1, in the spin coating process, the ZrO₂ sols were quickly coated on the surface of the stainless steel by a vacuum rotary coating machine; the ZrO₂ thin films were gradually formed through the homogenization and gelation of the ZrO₂ sols. Finally, the samples were dried for 30 min at 100 °C and then sintered for 5 h at 600 °C. ZrO₂ thin films with good performance were obtained.

1.2 Experimental tests and characterization

1.2.1 Film surface characterization

The phase composition of the ZrO₂ films was examined by Raman spectroscopy by a Renishaw InVia (Argon, 532 nm), and its phase composition was also determined by X-ray diffraction. Moreover, the surface chemical composition of the products was investigated by X-ray photoelectron spectroscopy (XPS), and the cross-sections of the coated specimens were obtained for thickness measurements. In addition, the surface morphologies of the samples were observed by an atomic force microscope (AFM) (CSPM4000 SPM, Benyuan).

1.2.2 Electrochemical tests

The electrochemical tests were carried out by an electrochemical workstation (CHI660C, Chenhua), including electrochemical impedance spectroscopy, potentiodynamic polarization testing technology and electrochemical noise technology. In the electrochemical tests, 1 cm² areas of the coated specimens and matrix samples were exposed as the electrochemical measurement surfaces, while other non-working surfaces were encapsulated with paraffin wax, and three electrode potentiodynamic scans were performed by the three aforementioned electrochemical technologies; when the electrochemical impedance spectroscopy and potentiodynamic polarization testing technology were used, the substrate samples or coated samples were the working

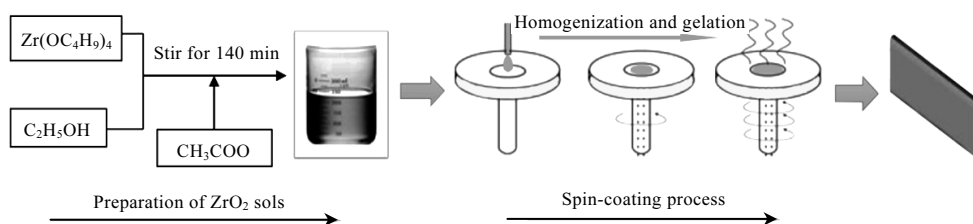


Fig.1 Preparation and spin coating process of ZrO_2 sols

electrode (WE), Pt was the counter electrode (CE), and Ag/AgCl was the reference electrode (RE); when the electrochemical noise technology was used, two coated samples were working electrode 1 (WE1) and working electrode 2 (WE2), and Ag/AgCl was the reference electrode (RE).

For the electrochemical impedance spectroscopy, the low frequency and high frequency of the experimental scanning was 0.01 Hz and 1×10^5 Hz, respectively. In the potentiodynamic polarization tests, the scanning rate was 10 mV/s, and the applied potential ranged from -2.0 to +3.0 V at a test temperature of 25 °C. When electrochemical noise technology was used, the sampling interval was 0.1 s, and the running time was 1200 s.

NaCl solutions with mass fractions of 0.5%, 2%, 3.5%, 5%, 6.5% and 8% were obtained from distilled water and analytically pure NaCl and were used as the corrosive media.

In the process of electrochemical testing, for the study of the solution temperature factor, electrochemical impedance spectroscopy (EIS) was used to study a coated specimen in 3.5% NaCl solutions with different solution temperatures. In addition, this technology was also used to investigate a bare substrate in 3.5% NaCl solutions of 25 °C. For the coated sample, the experimental solution temperatures were 25, 35, 38, 40, 45, 50, 55, 60, 65 °C. The coated sample was successively placed in the NaCl solutions with the nine aforementioned solution temperatures, and then, a series of electrochemical impedance spectroscopy was obtained for the coated specimen in each NaCl solution with different solution temperatures. After the electrochemical impedance spectroscopy tests, the coated sample surface was observed by optical microscope.

For the study of the NaCl concentration factor, electrochemical impedance spectroscopy (EIS) was used to study a coated specimen in NaCl solutions with various NaCl concentrations; the experimental temperature was 25 °C, and the NaCl concentrations (mass fraction) tested were 0.5%, 2%, 3.5%, 5%, 6.5% and 8%. The coated sample was successively placed in NaCl solutions with the six aforementioned NaCl concentrations, and then electrochemical impedance spectroscopy tests were performed. The coated sample was also observed by optical microscope. Based on the characteristics variation in the electrochemical impedance spectra

of the coated sample, electrochemical noise technology and potentiodynamic polarization experiments were used in NaCl solutions with concentrations of 2%, 3.5% and 5%, which further studied the corrosion properties of the coated sample and further determined the electrochemical characteristics of the coated sample in 2%, 3.5% and 5% NaCl solutions. Meanwhile, as a contrast, the matrix material was immersed in the three aforementioned NaCl solutions for potentiodynamic polarization experiments, and the polarization curves were measured. Before and after the experiment, the masses of the coated samples and matrices were determined.

1.2.3 Tribocorrosion tests

Linked with the tribometer and the electrochemical workstation, ZrO_2 and SiC ceramics were used as the friction pair materials. The contact form of the friction was ball/disc contact with a SiC ceramic grinding ball with a diameter of 5 mm; a pattern of reciprocating friction and wear was set, the experimental speed and load were 33 mm/s and 1.2 N, respectively, and three electrode potentiodynamic scanning parameters were scanning rate of 8.89 mV/s and applied potential ranging from -2.0 to +6.0 V at 25°C. The friction and electrochemical corrosion were applied simultaneously, and Tafel curves and diagrams of the friction coefficient were obtained to study the tribocorrosion properties of the coated samples in NaCl solutions of 2%, 3.5%, 5%, 6.5%. Moreover, the grinding marks were observed by a scanning electron microscope (SEM, S-4800, Hitachi). Before and after the experiment, and the masses of the coated samples and matrices were determined.

2 Results and Discussion

2.1 Film surface characteristics

2.1.1 XPS and phase analysis

Fig.2a is the XPS spectra of the ZrO_2 film on the sample surface. Compared with the corresponding standard electron binding energy, peak 1 and peak 2 at the binding energies of 182.2 and 184.6 eV, respectively, favorably indicate the chemical bonding of ZrO_2 ^[37]. Thus, ZrO_2 films are obtained on the substrate by the sol-gel spin coating process.

For the phase analysis of ZrO_2 films, XRD and Raman spectra were used. Fig.2c is the XRD pattern of the coated sample. Compared with the standard data, it is found that the

ZrO₂ film on the surface of the coated sample mainly consists of monoclinic and tetragonal phases. In order to further determine the phase composition of the film, Raman spectra was used to further analyze the ZrO₂ film.

Generally, there are three kinds of phases in ZrO₂ thin films, the monoclinic phase, tetragonal phase and cubic phase. The tetragonal phase corresponds to Raman peaks at 270, 315, 455, 602 and 645 cm⁻¹, and the monoclinic phase corresponds to Raman peaks at 192, 335, 347, 382, 476 (strong), 556, 617 and 638 cm⁻¹ [38]. Fig.2b is the Raman spectrum of the surface of the ZrO₂ film, which shows the spectral peaks of the monoclinic phase at 192 and 556 cm⁻¹ and those of the tetragonal phase at 270, 315 and 645 cm⁻¹. Accordingly, under the present experimental sintering technology, the main phase of ZrO₂ is the tetragonal phase with the existence of certain monoclinic

phases. Among these phases, tetragonal phase ZrO₂ possesses good expansion uniformity without mutation or brittle fracture^[39]. Furthermore, the presence of the tetragonal phase is vital for good corrosion and wear resistance of ZrO₂ thin films in service.

2.1.2 Surface morphology

The surface morphologies of the ZrO₂-coated sample are observed by optical microscope and SEM. As shown in Fig.3a, the surface has a color distribution of spots on the film surface. Based on the observations of the optical microscope, scanning electron microscopy (SEM) is used to further investigate the film surface. Fig.3b and Fig.3c are SEM images at different magnifications; the surface is smooth and flat at the micron scale, and at the nanometer scale, the particles are uniformly distributed, and the thin film has excellent compactness.

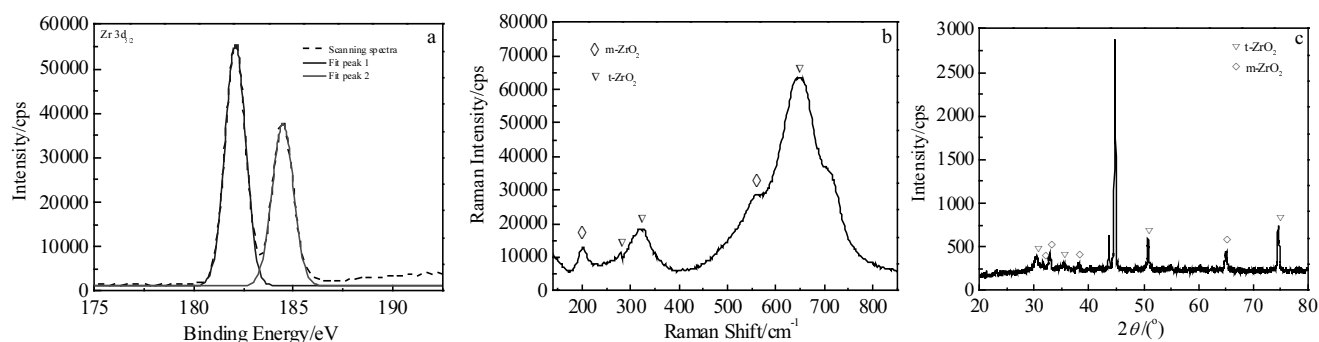


Fig.2 XPS spectra (a), Raman spectrum (b), and XRD pattern (c) of ZrO₂ films

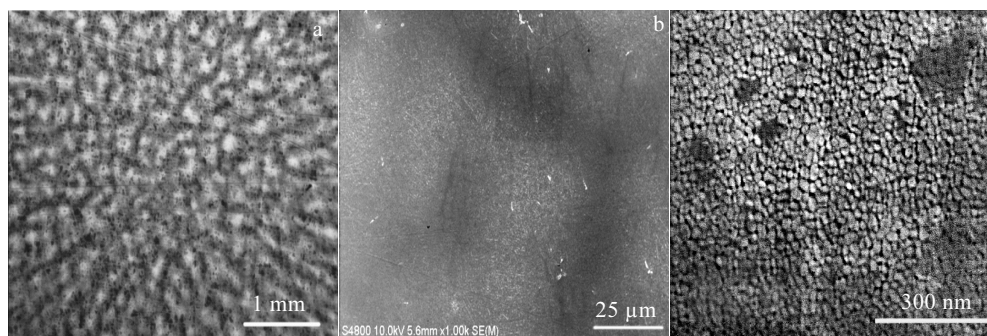


Fig.3 Surface morphologies of the ZrO₂ film: (a) optical image and (b, c) SEM images

The surface morphologies of the film are observed by atomic force microscopy (AFM). As seen in Fig.4 and Table 1, the average roughness (R_a) and root mean square roughness (RMS) of the film are obtained by image analysis software. In Fig.4, certain protrusions can be observed. Overall, the ZrO₂ film is deposited well on the surface of the substrate. In Table 1, the average surface roughness of the ZrO₂ thin film is 11.7 nm, and the film surface is flat and compact in Fig.3c.

2.1.3 Film thickness

For the coated sample through sintering molding, a cross-section of the sample is obtained by processing and

machining. Fig.5 is SEM image of the cross-section of the coated sample. The film thickness of the coated sample is approximately 340 nm.

2.2 Solution temperature factor analysis

In an electrolyte solution, the electrochemical characteristics of the coated sample vary at different temperatures. The solution temperature is one of the factors affecting the electrochemical process. Therefore, the electrochemical impedance spectroscopy of the coated sample in 3.5% NaCl solutions with solution temperatures ranging from 25~65 °C is used to study the influence of the solution temperature factor on the electrochemical characteristics, and the elec-

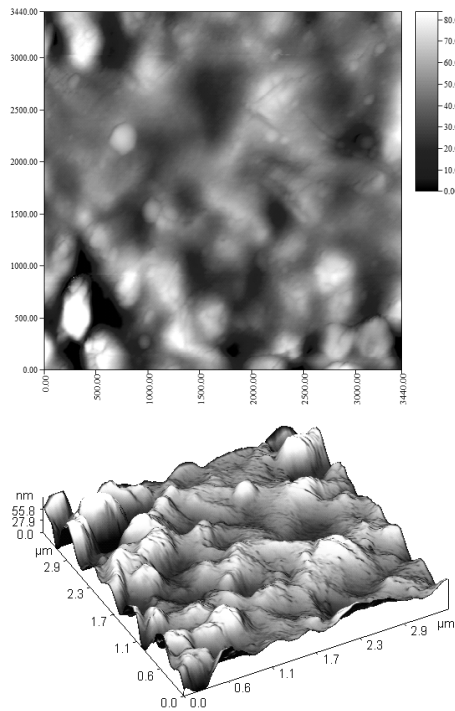


Fig.4 AFM morphologies of the ZrO₂ thin film

Table 1 Surface roughness of ZrO₂ thin film

Collection area	R_a/nm	RMS/nm
3440 nm×3440 nm	11.7	15.3

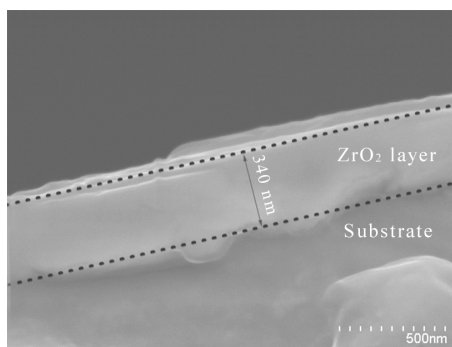


Fig.5 SEM image of the cross-section of the coated sample

Electrochemical impedance data are obtained, as shown in Fig.6. Fig.6a is the equivalent circuit diagram ($R_s(C_{coat}R_{coat})$ ($CPE(R_{ct}W)$)) corresponding to the electrochemical impedance spectroscopy of the coated sample at various solution temperatures. In the equivalent circuit diagram, R_s is the electrolyte solution resistance, C_{coat} is the ZrO₂ film capacitance, R_{coat} is the ZrO₂ film resistance, R_{ct} is the charge transfer resistance, CPE is the equivalent constant phase angle element in the process of charge transfer, and W is the

Warburg impedance in the process of charge transfer; these equivalent elements are connected in series and parallel according to the equivalent circuit in Fig.6.

Fig.6b shows the electrochemical impedance spectra of the coated sample in 3.5% NaCl solutions at different temperatures. As shown in Fig.6, the capacitive resistance arc at the moderate and high frequencies gradually decrease with the increase of the solution temperature. Fig.7 is the diagram of the electrochemical data fitting parameter of the coated samples at different temperatures. As shown in Fig.7a, the film resistance R_{coat} decreases with the increase of the solution temperature, which is consistent with the variation of the moderate and high frequency capacitive arc in Fig.7b, reflecting a decrease in the corrosion resistance of the ZrO₂ film. When the coated sample is immersed in the 3.5% NaCl solution, the chloride ions acceleratingly diffuse toward the inner part of the ZrO₂ film with the increase of the solution temperature, and the protective effect of the film is relatively weakened, accompanied by the adsorption of many more chloride ions at local sites of the passivation film, resulting in local damage of the passivation film. Accordingly, in the damage position, the matrix acts as an anode; correspondingly, a cathode is formed outside the ZrO₂ film, and the following electrochemical processes occur inside and outside the film^[40]:

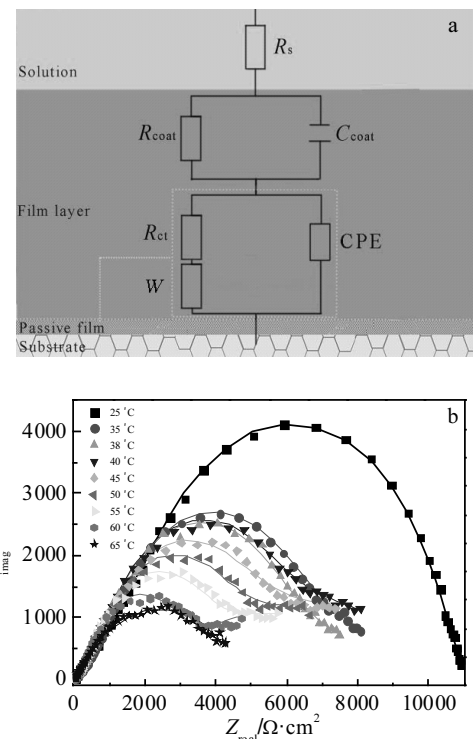
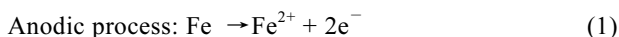


Fig.6 Electrochemical impedance spectroscopy of the coated specimen in the 3.5% NaCl solution: (a) equivalent circuit and (b) Nyquist diagram at the solution temperature of 25~65 °C



At the electrochemical reaction site, Fe^{2+} separates from the anode and further reacts with OH^{-} in the electrochemical medium, i.e., the following reaction process:



In a NaCl electrolyte solution, the presence of chloride ions is beneficial to the electrochemical corrosion process. Fig.7b is a graph of the charge transfer resistance at different solution temperatures, which shows that the charge transfer resistance increases with the increase of the solution temperature. In Fig.7c, the Warburg impedance greatly fluctuates with variation of the solution temperature. Overall, the fluctuation of Warburg impedance trends downward, and the value of the second fluctuation peak is smaller than that of the first fluctuation peak. Beyond a solution temperature of 55 °C, the fluctuation of the Warburg impedance is stable at a lower level. The trends are distinct in the charge transfer resistance and Warburg impedance with solution temperature. Indeed, the solution temperature affects the electrochemical reaction rate, oxygen content and diffusion in the solution.

As the coated sample is immersed in the 3.5% NaCl solution, the chloride ions gradually penetrate the film, and then contact the substrate with further electrochemical reaction, and the electrochemical process is mainly oxygen absorption corrosion. With the increase of the solution temperature, the rate of the electrode reaction increases. Moreover, the amount of reaction products formed increases, and iron hydroxides are located at tiny corrosion sites, hindering the charge transfer; thus, the charge transfer resistance R_{ct} increases gradually.

Meanwhile, increasing solution temperature decreases the solubility of oxygen in the NaCl solution, and the cathodic process in the corrosion area is affected. Below a solution temperature of 38 °C, the oxygen content in the electrolyte solution is sufficient; with the increase of the solution temperature, the adsorption of chloride ion increases at the corrosion site, the electrochemical reaction process accelerates, and the Warburg impedance increases,

which is positively related to the reaction rate. As shown in Fig.7c, the first fluctuation peak appears.

The lower the Warburg impedance is, the higher the diffusion rate is, and the slower the corrosion rate is because the diffusion controls the corrosion. Above a solution temperature of 38 °C, with the increase of the solution temperature, the oxygen content gradually decreases, the cathodic process slows and the Warburg impedance decreases; new corrosion sites are gradually formed on the surface of the coated specimen. At new corrosion sites, the corrosion rate increases with solution temperature, and the Warburg impedance increases; moreover, the second wave peak appears, as seen in Fig.7c. As the solution temperature exceeds 55 °C, the oxygen content in the electrolyte solution is at a lower level, the rate of oxygen absorption corrosion slows, and the Warburg impedance steadily fluctuates near a lower value.

The electrochemical characteristics of the coated sample in NaCl solutions at various solution temperatures were analyzed by electrochemical impedance spectroscopy. To observe the surface characteristics of the coated specimen after testing, the surface morphology of the coated specimen was investigated by optical microscopy. Fig.8 shows optical microscopic images of the surface of a coated sample after electrochemical impedance spectroscopy testing. In Fig.8a, cracks and certain corrosion spots appear on the surface of the coated sample. Fig.8b shows a corrosion hole caused by electrochemical corrosion. Although different types of failure characteristics are exhibited on the specimen surface, obvious destruction phenomenon emerges in certain regions of the surface film; as shown in Fig.8c, most areas of the ZrO_2 film remain intact after the electrochemical experiments. In the 3.5% NaCl solutions, with the increase of the solution temperature, the heat resistance decreases on the film surface of the local sample area, and the appearance of local cracks indicates that there is slight thermal fatigue on the surface; moreover, the local corrosion is dominated by pitting in the immersion process, as shown by the corrosion holes on the surface. Therefore, in the 3.5% NaCl solutions, the continuous increase of the solution temperature

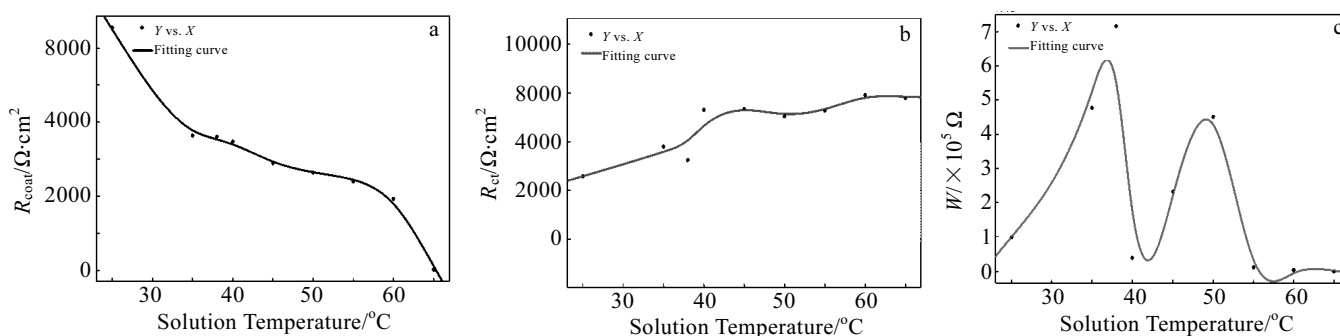


Fig.7 Electrochemical data fitting parameter of the coated sample at different temperatures: (a) R_{coat} , (b) R_{ct} , and (c) W

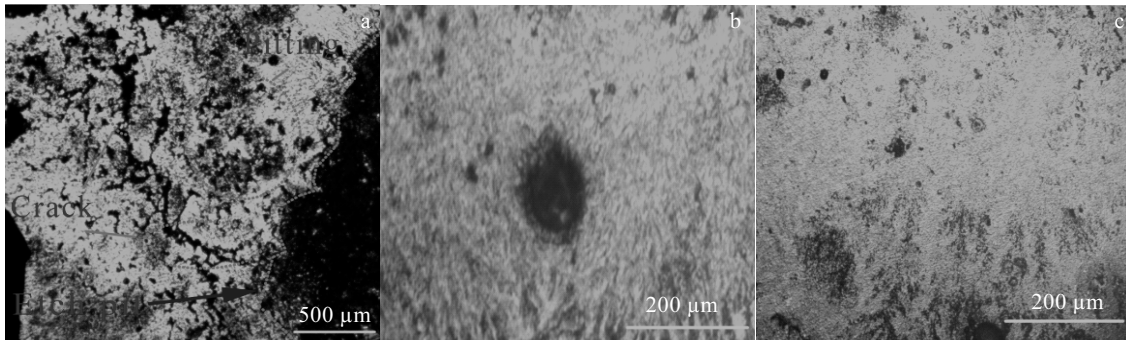


Fig.8 OM images on the surface of the coated sample after electrochemical impedance spectroscopy tests: (a) destruction area, (b) the corrosion hole, and (c) undamaged area

eventually leads to the appearance of local cracks and corrosion holes on the surface of the coated sample.

2.3 Solution concentration factor study

2.3.1 Electrochemical impedance spectroscopy (EIS) analysis

For a coated sample immersed in NaCl solution, the electrolyte concentration also affects the occurrence of the electrochemical process. Accordingly, in the study of the electrolyte concentration factor, the solution temperature is constant at 25 °C, and the experimental electrolyte concentration ranges from 0.5%~8%. Fig.9 is the electrochemical impedance spectroscopy and the equivalent circuit diagram of the coated sample in 0.5%~8% NaCl solutions. Fig.10 is the electrochemical data fitting parameter diagram of the coated sample in 0.5%~8% NaCl solutions. As shown in Fig.9a, in the equivalent circuit diagram ($R_s(C_{coat}R_{coat})(CPE R_{pass})$), R_s is the solution resistance, C_{coat} is the film capacitance, R_{coat} is the film resistance, R_{pass} is the passive film resistance, and CPE is the corresponding equivalent constant phase angle element. In Fig.9b, the capacitance arc at high frequency decreases gradually with increasing NaCl concentration, which is consistent with the trend of the film resistance R_{coat} in Fig.10a.

In Fig.10b, the passive film resistance R_{pass} first decreases and then increases with NaCl concentration, and there is a minimum near the concentration of 3.5% which may be related to the variation of the oxygen content in the electrolyte solution. In the electrolyte solution, the augmentation of the NaCl concentration also reduces the oxygen content in the solution. When the NaCl concentration is less than 5%, the oxygen content changes minimally with the concentration, while the oxygen depolarization process gradually accelerates, and the passive film is continuously destroyed at the corrosion site, resulting in the decrease of the passive film resistance R_{pass} . Beyond NaCl concentration of 5%, with the increase of the NaCl concentration, the oxygen content obviously decreases in the electrolyte solution;

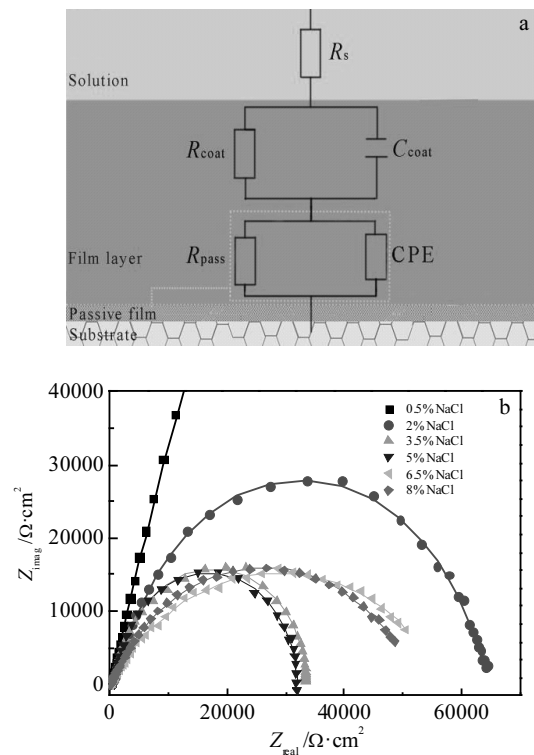


Fig.9 Electrochemical impedance spectroscopy of the coated specimen in the different NaCl solutions: (a) equivalent circuit and (b) Nyquist diagram at the solution concentration of 0.5%~8%

the oxygen depolarization process is inhibited, the passive film can be repaired, and the resistance R_{pass} progressively increases.

The surface morphologies of the coated sample was observed after the electrochemical impedance spectroscopy (EIS) tests. Fig.11 shows optical microscope images of the surface morphology of the coated sample after the EIS tests. In Fig.11a, for the coated samples, the surfaces are corroded by chloride ions in different NaCl solutions with continuous electrochemical reaction processes, and obvious corrosion

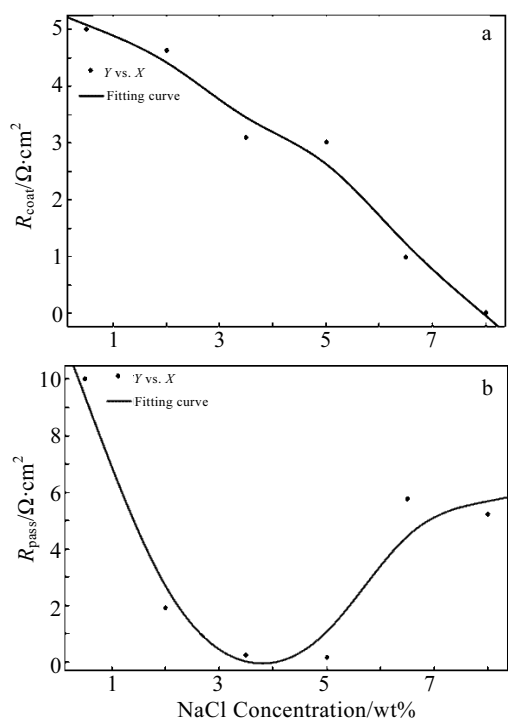


Fig.10 Electrochemical data fitting parameter of the coated sample with different NaCl concentrations: (a) R_{coat} and (b) R_{pass}

holes ultimately appear on the surfaces of the coated specimens, but no significant corrosion characteristics are found in most areas, as shown in Fig.11b. Therefore, in the NaCl solution, with increasing NaCl concentration, slight pitting corrosion occurs on the surface of the coated specimen.

2.3.2 Electrochemical noise study

The study of electrolyte concentration factor shows that the passive film resistance R_{pass} has a turning variation in the concentration range of 2%~5%. Based on the above changing feature, electrochemical noise technology and potentiodynamic polarization tests are used to investigate the changing electrochemical characteristics. Fig.12 is the time domain diagrams of the coated samples immersed in 2%, 3.5% and 5% NaCl solutions. With the increase of the NaCl concentration, obvious noise peaks gradually appear in the time domain diagram, and the appearance of noise peaks indicates the occurrence of electrochemical corrosion. In the 2% NaCl solution, as shown in Fig.12, a small noise peak appears when the sample is immersed for 600~800 s. For the coated sample tested in the 3.5% NaCl solution, as seen in Fig.12, a large noise peak appears in the initial stage of immersion, with the potential fluctuating steadily after recovery, reflecting the existence of obvious electrochemical corrosion during the immersion process.

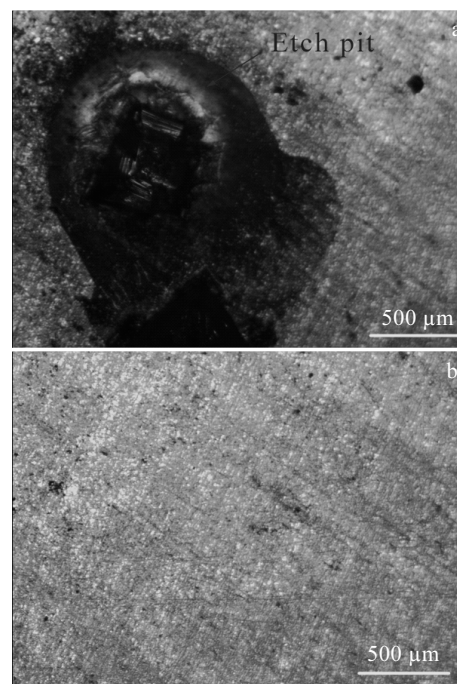


Fig.11 OM images on the surface of the coated sample after electrochemical impedance spectroscopy tests: (a) pitting corrosion and (b) undamaged area

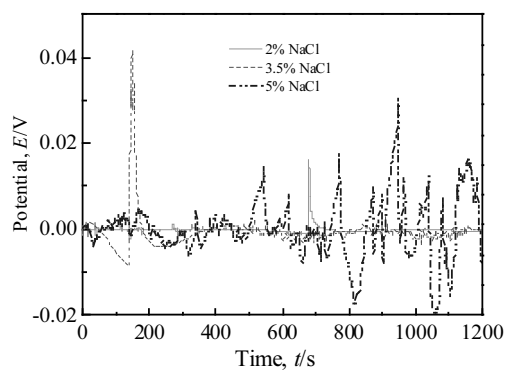


Fig.12 EN diagrams of the coated specimen immersed in 2%, 3.5%, 5% NaCl solutions

When the NaCl concentration continues to increase, the corrosion is more significant and the fluctuations in the potential progressively increase. For the coated sample immersed in the 5% NaCl solution, Fig.12 shows a slight potential fluctuation in the initial stage of immersion, and a larger potential fluctuation slowly emerges in the latter stage. Therefore, when the NaCl concentration varies from 2% to 5%, the potential fluctuation is more obvious, and the corrosion is more significant, which further explains the trend of the electrochemical impedance spectroscopy in the concentration range of 2%~5% in Fig.9b.

2.3.3 Potentiodynamic polarization analysis

Fig.13a and Fig.13b are the Tafel curves of the bare matrix and the coated specimen at NaCl concentrations of 2%, 3.5% and 5%, respectively. From these figures, the corrosion potential of the aforementioned samples increases with the increase of the NaCl concentration, and the electrochemical corrosion becomes more prone to proceed. In Fig.13b, the current density i_p in the passivation region of the Tafel curve increases with the concentration, i.e., $i_p-2\% < i_p-3.5\% < i_p-5\%$, and the passivation ability of the coated samples decreases, further confirming decrease of the passive film R_{pass} in Fig.10a. Moreover, as labeled in Fig.13b, the breakdown potential E_b of the coated sample is greater than zero in the 2% and 3.5% NaCl solutions. Fig.13c is the corrosion current density of the bare matrix and the coated specimen at NaCl concentrations of 2%, 3.5% and 5%. When the experimental samples are immersed in electrolyte solution, electrochemical corrosion occurs on the surface with the generation of the corrosion current. In Fig.13c, these corrosion current densities present a similar increase with the increase of the NaCl concentration. The corrosion current density of the matrix is greater than that of the coated specimen. Fig.13d is the mass loss of the bare matrix and the coated specimen before and after the experiment at

NaCl concentrations of 2%, 3.5% and 5%, which shows an increase in the mass loss with the increase of the NaCl concentration. The mass loss of the matrix is greater than that of the coated specimen, which is consistent with the trend of the corrosion current, indicating that the electrochemical corrosion becomes more serious with the increase of the NaCl concentration.

The above evidence shows that corrosion resistance of the coated specimen is better than that of the bare matrix, and when the NaCl concentration varies from 2% to 5%, the corrosion current increases, and the electrochemical corrosion becomes more serious, which corresponds to the decrease in the film resistance R_{coat} of the coated specimen with the increase of the NaCl concentration, as shown in Fig.10a.

2.4 Tribocorrosion behavior

2.4.1 Electrochemical characteristics and friction coefficient

Combined with the above analysis, NaCl concentrations of 2%, 3.5%, 5% and 6.5% were used to investigate the tribocorrosion behavior of the matrix and the coated samples, and the properties of the ZrO_2 films were further evaluated. Fig.14 shows the Tafel curves of the matrix during tribocorrosion tests of the four aforementioned

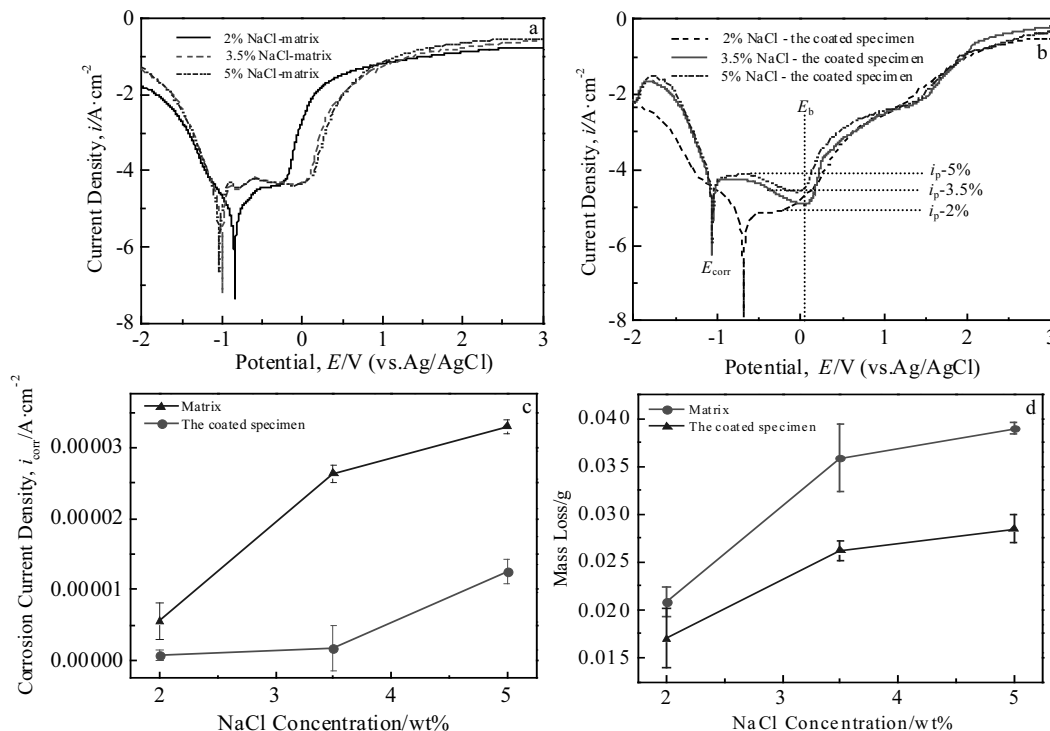


Fig.13 Potentiodynamic polarization curves in 2%, 3.5% and 5% NaCl solution recorded on the matrix (a) and the coated specimens (b); corrosion current density (c) and the mass loss (d) of the matrix and the coated specimens measured in 2%, 3.5% and 5% NaCl solutions

NaCl solutions, and Table 2 is the electrochemical parameters obtained from the polarization curves of the substrates during the tribocorrosion tests in the NaCl solutions. Combined with the Tafel curves in Fig.14, as shown in Table 2, when the NaCl concentration increases from 2% to 6.5%, the corrosion current density of the matrix increases, and the absolute value of corrosion potential increases; thus, electrochemical corrosion is more prone to occur during the tribocorrosion process.

Fig.15 shows the potentiodynamic polarization curves of the coated specimens and the corresponding corrosion current density and corrosion potential during tribocorrosion tests in 2%, 3.5%, 5% and 6.5% NaCl solutions. Fig.15b shows the corrosion current densities and potentials obtained from the Tafel curves of Fig.15a. In Fig.15b, with the increase of the NaCl concentration in the range of 2% to 6.5%, the corrosion current density of the coated samples increases and the corrosion potential decreases during the tribocorrosion process, which is consistent with the trends of the substrates. Moreover, as labeled in Fig.15a, the breakdown potential E_b is less than zero, but the breakdown potential E_b is greater than zero in Fig.13b for the single electrochemical corrosion, i.e., $E_{b-tribocorrosion} < E_{b-corrosion}$, illustrating that pitting corrosion is more prone to occur during tribocorrosion than during the single corrosion process of the coated specimens.

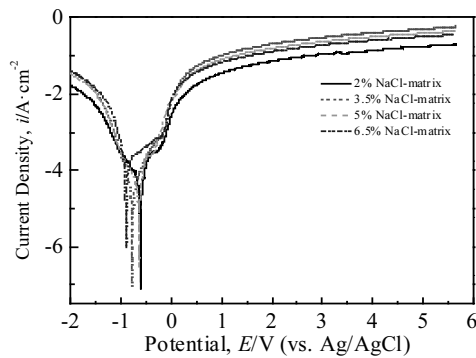


Fig.14 Potentiodynamic polarization curves of substrates during tribocorrosion test in 2%, 3.5%, 5% and 6.5% NaCl solution

Table 2 Electrochemical parameters of substrates during tribocorrosion test

NaCl concentration/wt%	Corrosion potential, E_{corr}/V	Corrosion current, $i_{corr}/\times 10^{-5} A \cdot cm^{-2}$
2	-0.61828	2.8734
3.5	-0.78016	5.9366
5	-0.64482	9.8616
6.5	-0.90983	29.81

Fig.16a is the mass loss of the matrix and the coated specimens in the process of tribocorrosion under the four aforementioned NaCl concentrations. Fig.16b is the friction coefficient of the matrix and the coated specimen during tribocorrosion in different NaCl solutions. From Fig.16a, the mass losses of the matrix and the coated specimen increase with the increase of the NaCl concentration, and the mass loss of the matrix is greater than that of the coated specimen, providing additional evidence that more serious tribocorrosion occurs on the surface of the matrix compared with the coated specimen.

As shown in Fig.16b, the average friction coefficient of the matrix has an increasing trend, but the minimum of the average friction coefficient appears for the sample in the 3.5% NaCl solution. According to the electrochemical impedance spectroscopy analysis based on the solution concentration factor, as shown in Fig.10b, the passive film resistance R_{pass} reaches a minimum near the concentration of 3.5% NaCl, corresponding to the minimum of the average friction coefficient of the matrix during tribocorrosion. The two sides or protruding parts on the outer edges of the grinding marks produced by abrasive wear are strong areas of plastic deformation in the 3.5% NaCl solution^[41] and are removed by the accelerating electrochemical corrosion during the process of friction and wear; thus, the average friction coefficient decreases during the tribocorrosion of the matrix in the 3.5% NaCl solution.

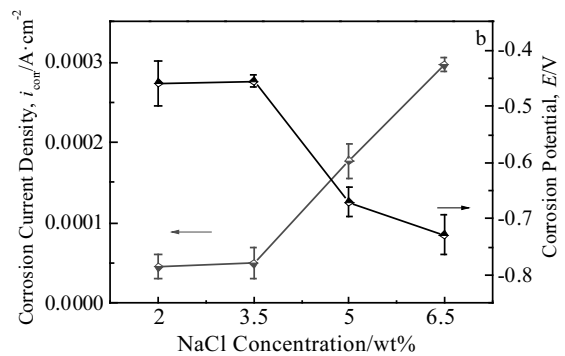
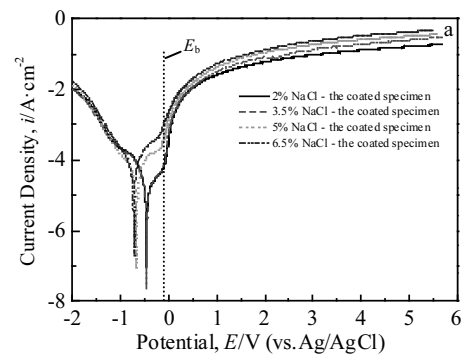


Fig.15 Potentiodynamic polarization curves of the coated specimens (a) and the related corrosion current density and potential during tribocorrosion test in 2%, 3.5%, 5% and 6.5% NaCl solutions (b)

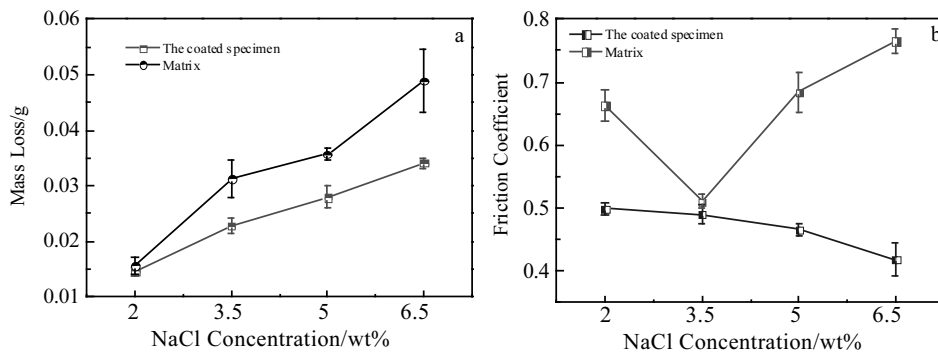


Fig.16 Mass loss (a) and friction coefficient (b) of matrix and the coated specimens during tribocorrosion test in different concentrations NaCl solution

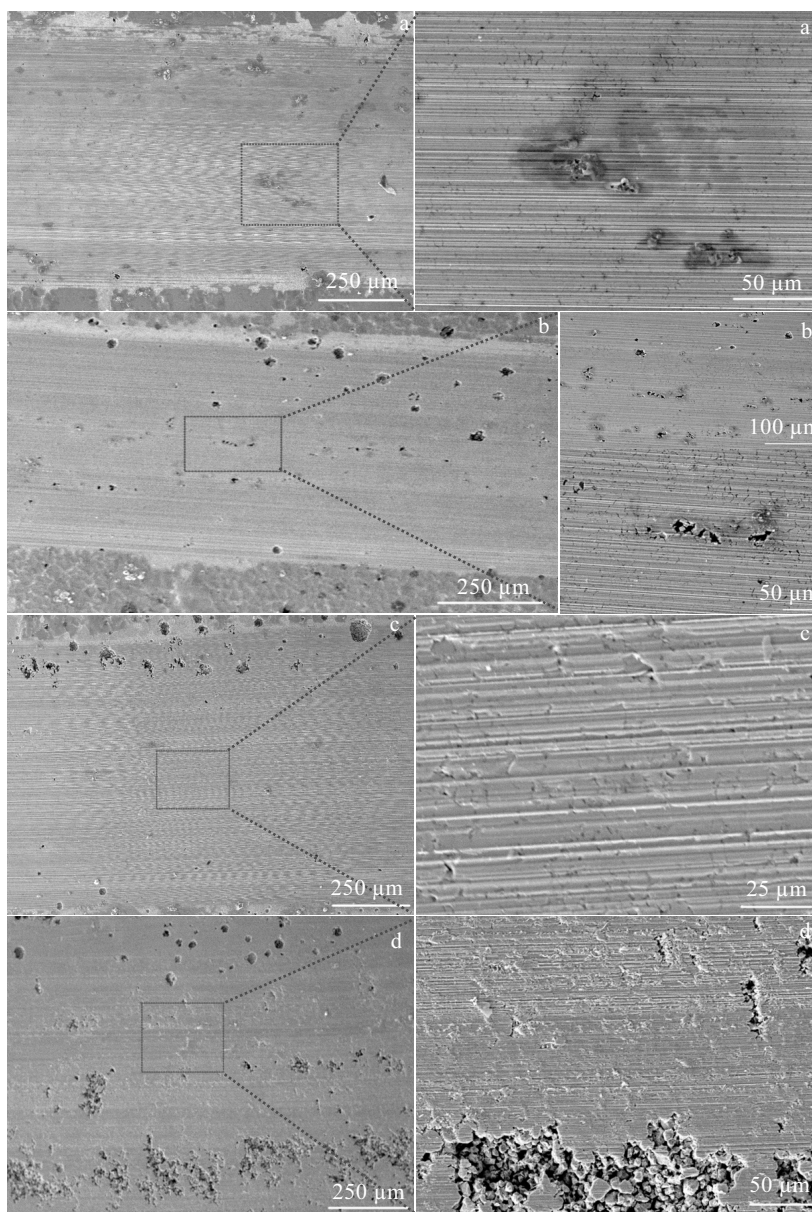


Fig.17 SEM images of the grinding marks of the coated specimens during tribocorrosion test performed in 2% (a, a'), 3.5% (b, b'), 5% (c, c'), and 6.5% NaCl solution (d, d')

For the coated samples, in Fig.16b, the corresponding average friction coefficient decreases. From Fig.16a, the existence of the ZrO_2 films reduces the material loss and has a protecting effect on matrix; furthermore, with the increase of the NaCl concentration, the protruding areas on the surface are prone to removal by electrochemical corrosion, which may be the reason for the decrease in the average friction coefficient of the coated specimen during tribocorrosion.

2.4.2 Wear morphologies during tribocorrosion

Under the coupled conditions of electrochemical corrosion and wear, the grinding mark morphologies of the coated specimens were distinguished at different NaCl concentrations. Fig.17a~17d are the morphologies of the grinding marks of the coated specimens in the 2%, 3.5%, 5% and 6.5% NaCl solutions, respectively. In Fig.17a, as seen in the red marked area, an aggregation of corrosion holes appears in the center of the grinding mark, linear scotches are produced on the grinding mark, and pitting corrosion and abrasive wear occur on the surface. In the 3.5% NaCl solution, as shown in Fig.17b, obvious corrosion holes appear on the edges of the grinding mark, and a series of tiny corrosion pits exist in the center; as indicated in the red marked area, obvious pitting corrosion is gradually aggravated, indicating that pitting corrosion is more prone to occur during tribocorrosion, which is corresponding to the negative breakdown potential E_b of the coated sample during the tribocorrosion from Fig.15a. Currently, corrosion wear becomes more serious with significant abrasive wear in the 3.5% NaCl solution.

As shown in Fig.17c, linear scotches still appear in the wear area with the appearance of microcracks and shedding of surface material, and obvious adhesive wear begins to appear. Thus, the wear evolves into abrasive wear, adhesion wear and corrosion wear under an NaCl concentration of 5%. With the increase of the NaCl concentration, due to the synergistic effects of electrochemical corrosion, the wear is aggravated, and the amount of wear debris increases. When the NaCl concentration increases to 6.5%, as shown in Fig.17d and its enlarged graphs, obvious microconvex bodies exist on the surface because of the accumulated wear debris; accompanied by furrows and scratches on the surface, the adhesion wear is even more obvious. Furthermore, for the coated specimen, the tribocorrosion process is mainly dominated by abrasive wear, adhesion wear and corrosion wear.

3 Conclusions

1) For the solution temperature factor, in the range of 25~65 °C, the resistance to electrochemical corrosion decreases with the solution temperature for the coated sample, after electrochemical impedance spectroscopy experiments at various solution temperatures, serious pitting corrosion and

obvious cracks exist on the surface of the coated specimen.

2) Within the concentration range of 0.5%~8%, the chloride ion attack is hindered by the ZrO_2 film, but the protective effect of the film weakens with the increase of the NaCl concentration. Furthermore, pitting corrosion appears on the surface of the coated specimen after electrochemical impedance spectroscopy experiments at different NaCl concentrations.

3) The presence of the ZrO_2 films reduces the material loss caused by tribocorrosion and single electrochemical corrosion compared with that of the bare matrix.

4) Compared with single electrochemical corrosion, pitting corrosion is more prone to occur in the process of tribocorrosion. Under the synergistic action of electrochemical corrosion and wear of the coated sample, the wear mechanisms are mainly abrasive wear, adhesion wear and corrosion wear. Increasing the NaCl concentration from 2% to 6.5%, the abrasive wear is more significant, and corrosion wear are aggravated at higher concentrations with the existence of adhesion wear.

References

- [1] Bhuiyan S, Law D W, Nicholls P et al. *Construction & Building Materials*[J], 2018, 162: 503
- [2] Wei X, Zhang C, Ling X. *Journal of Alloys & Compounds*[J], 2017, 723: 237
- [3] Qi X, Mao H, Yang Y. *Corrosion Science*[J], 2017, 120: 90
- [4] Delaunoi F, Tshimombo A, Stanciu V et al. *Corrosion Science*[J], 2016, 110: 273
- [5] Liu M, Duan D L, Jiang S L. *Acta Metallurgica Sinica*[J], 2018, 31: 1049
- [6] Yan Y, Neville A, Dowson D. *Tribology International*[J], 2006, 39: 1509
- [7] Voevodin A A, Zabinski J S. *Composites Science & Technology* [J], 2005, 65: 741
- [8] Mischler S. *Tribology International*[J], 2008, 41: 573
- [9] Shan X, Wei L Q, Liu P et al. *Ceramics International*[J], 2014, 40: 12 327
- [10] Mondal J, Marques A, Aarik L et al. *Corrosion Science*[J], 2016, 105: 161
- [11] Lee S H, Woo S P, Kakati O et al. *Surface & Coatings Technology*[J], 2016, 303: 162
- [12] Wang H, Sun T, Chang L et al. *Surface & Coatings Technology*[J], 2017, 325: 136
- [13] Ćurković L, Ćurković H O, Salopek S et al. *Corrosion Science* [J], 2013, 77: 176
- [14] Yeh T K, Chien Y C, Wang B Y et al. *Corrosion Science*[J], 2008, 50: 2327

- [15] Luo H, Cai Q, Wei B et al. *Journal of Alloys and Compounds*[J], 2009, 474: 551
- [16] Duan Z, Luo D, Liu Z et al. *Ceramics International*[J], 2017, 43: 5089
- [17] Li H, Liang K, Mei L et al. *Journal of Materials Science Letters*[J], 2001, 51: 320
- [18] Wang J, Su M Y, Qi J Q et al. *Sensors & Actuators B Chemical*[J], 2009, 139: 418
- [19] Encinas-Sánchez V, Macías-García A, Pérez F J. *Ceramics International*[J], 2017, 43: 13 094
- [20] Hao S J, Wang C, Liu T L et al. *International Journal of Hydrogen Energy*[J], 2017, 42: 29 949
- [21] Ratnayake S P, Silva N D, Kaupuge T K et al. *Materials Science & Engineering B*[J], 2018, 229: 59
- [22] Garg N, Mittal V K, Bera S et al. *Thin Solid Films*[J], 2013, 545: 222
- [23] Tiwari S K, Tripathi M, Singh R. *Corrosion Science*[J], 2012, 63: 334
- [24] Kessman A J, Ramji K, Morris N J et al. *Surface & Coatings Technology*[J], 2009, 204: 477
- [25] Sui J H, Cai W. *Nuclear Inst & Methods in Physics Research B*[J], 2006, 251: 402
- [26] Obadele B A, Andrews A, Olubambi P A. *Wear*[J], 2015, 328: 295
- [27] Obadele B A, Lepule M L, Andrews A et al. *Tribology International*[J], 2014, 78: 160
- [28] Zhang W, Ji G, Bu A et al. *ACS Applied Materials & Interfaces*[J], 2015, 7: 28 264
- [29] Jouili M, Andrieux M, Ribot P et al. *Journal of Nanoscience & Nanotechnology*[J], 2011, 11: 8009
- [30] Tsai T, Barnett S A. *Journal of the Electrochemical Society*[J], 1995, 142: 3084
- [31] Kao A S, Gorman G L. *Journal of Applied Physics*[J], 1990, 67: 3826
- [32] Liu Senhui, Li Chengxin, Zhang Huiyu et al. *Scripta Materialia*[J], 2018, 153: 73
- [33] Norouzi M, Garekani A A. *Ceramics International*[J], 2014, 40: 2857
- [34] Verma K, Chaudhary B, Kumar V et al. *Vacuum*[J], 2017, 146: 524
- [35] Lee H S, Ng S S, Yam F K. *Vacuum*[J], 2018, 155: 16
- [36] Fong C Y, Ng S S, Yam F K et al. *Vacuum*[J], 2015, 119: 119
- [37] Yu J, Ji G, Liu Q et al. *Surface and Coatings Technology*[J], 2017, 331: 21
- [38] Noda L K, Gonçalves N S, S M D. *Vibrational Spectroscopy*[J], 2007, 44: 101
- [39] Lin Z H, Lin G, Wu L. *Chinese Journal of Rare Metals*[J], 2003, 27: 49
- [40] Yu J, Ji G, Shi Z et al. *Journal of Alloys and Compounds*[J], 2019, 783: 371
- [41] Zhang Z, Ji G, Shi Z. *Surface and Coatings Technology*[J], 2018, 350: 128

不锈钢表面溶胶-凝胶 ZrO₂ 膜在不同 NaCl 水溶液中的电化学腐蚀和摩擦腐蚀性能

张镇华, 冀国俊

(内蒙古工业大学 化工学院, 内蒙古 呼和浩特 010051)

摘要: 采用溶胶-凝胶旋涂法在 304 不锈钢基体上制备了 ZrO₂ 薄膜。采用电化学测试技术和往复磨损试验装置, 研究了薄膜在不同 NaCl 溶液中的电化学腐蚀和摩擦腐蚀性能。结果表明, 涂层试样的耐蚀性和摩擦学性能均优于裸露基体。在 NaCl 溶液中, 提高溶液温度或溶液浓度均降低了 ZrO₂ 薄膜的保护效果; 基于溶液温度因素的研究表明, 涂层试样表面出现严重的点蚀和明显的开裂; 基于溶液浓度因素的研究表明, 试样表面存在点蚀。对于涂层试样的摩擦磨损, 随着 NaCl 浓度从 2% 增加到 6.5%, 磨损更加明显, 腐蚀磨损加剧。

关键词: ZrO₂ 薄膜; NaCl 溶液; 电化学腐蚀; 摩擦腐蚀

作者简介: 张镇华, 男, 1990 年生, 硕士, 内蒙古工业大学化工学院, 内蒙古 呼和浩特 010051, 电话: 0471-6575722, E-mail: 1052745116@qq.com